MYU Tokyo

S & M 4556

Cloud-based Workplace Safety System Using Multi-algorithm Integrated Sensor Data Fusion

Shiau-Jing Ho,[1] Min-Jain Lee,[2] Wen-Ping Chen,[2] and Hui-Ping Tseng[1*]

[1]Department of Civil Engineering, College of Engineering, National Taiwan University, No. 1, Sec. 4, Roosevelt Rd., Taipei 106319, Taiwan (R.O.C)
[2]Department of Electrical Engineering, National Kaohsiung University of Science and Technology, No. 415, Jiangong Rd., Sanmin Dist., Kaohsiung City 807618, Taiwan (R.O.C)

(Received May 11, 2026; accepted July 2, 2026)

Keywords: work safety helmet, IoT, personnel positioning, multi-dimensional positioning

High-risk work environments expose personnel to dangerous accidents under rapidly changing conditions. Existing worker localization methods using RF identification, Wireless Fidelity (Wi-Fi), Bluetooth, or ultra-wideband (UWB) present tracking errors and instabilities caused by uneven anchor distribution or multipath interference. Additionally, current systems rarely integrate robust localization with automated multi-modal alerting. To address these limitations, we developed a cloud-based occupational safety system combining a custom safety helmet, UWB transceivers, and real-time IoT protocols. For precise tracking, an integrated data fusion framework blends enhanced trilateration, enhanced nonlinear least squares, and multi-circle overlap methods. A field test involving 120 participants across 150 independent trials was conducted in a 450 m^2 concrete atrium with obstructions. The results showed that the multi-algorithm fusion model achieved submeter localization accuracy, filtering out spatial jumps. The results contribute to the development of cellular UWB anchor grid scaling and modular sensor bus expansion. By demonstrating how raw micro-sensor data streams and dynamic geofencing can be integrated onto a unified edge-to-cloud layout, a wearable safety gear can be transformed from passive positioning trackers into active, intelligent hazard-mitigation instruments suitable for complex industrial sites.

1. Introduction

Traditional safety measures, such as warning signs, periodic training, and manual inspections, have played an important role in accident prevention. However, their passive nature and lack of real-time responsiveness have become increasingly evident in the workplace. In emergencies, conventional methods fail to immediately provide data regarding the location of affected personnel or the hazardous environment. Such delays prevent workers from issuing timely alerts and hinder rescue operations, often resulting in missed opportunities for effective intervention.

*Corresponding author: e-mail: wpc@nkust.edu.tw
https://doi.org/10.18494/SAM6410

ISSN 0914-4935 © MYU K.K.
https://myukk.org/

As work environments become complex, advanced wearable technologies with cloud computing offer new opportunities for workplace safety. However, systems currently used in the workplace are fragmented. Although smart safety systems are widely applied, few provide integrated solutions combining cloud-based management with emergency alert capabilities based on sensor technology. Most systems adopt single technologies to respond to specific risks, which necessitates a better coordination of personnel positioning, multi-modal monitoring, and cloud-based site management. In environments with severe signal obstruction, such systems present considerable localization errors and transmission stability.

The feasibility of embedding sensors into safety gear has already been proven, but their applications remain specialized. Forsyth *et al.* developed a system to monitor carbon monoxide poisoning by embedding pulse oximetry sensors into helmets, demonstrating high accuracy in detecting physiological distress.(1) Recently, a smart safety helmet with accelerometers and gyroscopes has been proposed to detect falls or fainting, transmitting alerts through a global system for mobile communication modules.(2) To prevent collision risks with heavy machinery in the workplace, a radio frequency identification (RFID)-based tracking system is introduced, achieving localization accuracy within 1 m.(3) Physiological and ultrasonic modules using Bluetooth(4) and IoT with LoRa communication and Kalman filtering are also implemented into the safety gear to improve the accuracy of abnormal motion detection.(5)

Beyond its superior decimeter-level spatial resolution, ultra-wideband (UWB) technology provides advantages over conventional narrowband wireless protocols such as Wi-Fi and Bluetooth Low Energy, making it well-suited for industrial environments. Because UWB transmits sub-nanosecond RF pulses across a wide bandwidth (≥499.2 MHz), it presents strong immunity to multipath propagation and severe signal fading commonly encountered around steel frameworks and concrete structures. The receiver effectively isolates the direct line-of-sight signal from delayed reflections, which is not found in narrowband continuous-wave systems.(6) Moreover, UWB employs precise time-of-flight measurements reinforced by physical-layer security mechanisms such as scrambled timestamp sequences, mitigating ranging spoofing and relay attacks that often compromise conventional received signal strength indicators or phase-based positioning frameworks.(7) Finally, its exceptionally low power spectral density, lower than −41.3 dBm/MHz, enables UWB signals to transmit on the noise floor of other active transmission networks without causing electromagnetic interference to nearby communication channels or crane telemetry modules.(8)

In this study, we developed a wearable monitoring and alert system for construction sites by integrating sensors, IoT, and cloud technologies to balance worker safety with usability and cost-effectiveness. The system is developed for multi-algorithm UWB precision localization, real-time cloud geofencing, and bidirectional audio broadcasting alerts on a unified platform for multi-functional hazard mitigation. The system integrates diverse sensing technologies (physiological, environmental, and positional) into a single, scalable cloud platform and operates on an integrated positioning algorithm to enhance the timeliness and accuracy of worker localizations in high-risk working environments where signals are often obstructed. On the management interface, the status and historical records of workers are tracked, supporting event assessment and rapid emergency response. Through the integration of sensing technology, the system offers a responsive, data-rich management platform to reduce workplace accidents in hazardous working environments.

2. System Architecture

2.1 System layer

We developed a smart safety monitoring system that integrates on-site sensing devices, positioning modules, cloud servers, and front-end interfaces. The developed system provides real-time worker positioning, abnormal state monitoring, and automated alerting functions. Its architecture comprises (1) sensing data acquisition, (2) communication and data transmission, (3) information management and visualization, and (4) cloud-based data processing layers.

2.1.1 Sensing data acquisition layer

This layer collects and transmits sensor data from the smart safety helmet to the microcontroller unit (MCU). The layer operates on UWB sensing technology, which measures the distance between the helmet wearer and nearby access points (APs). UWB technology was selected for its high transmission rate, strong anti-interference capability, and superior positioning accuracy, particularly in construction environments with multipath effects and obstructions.(9,10) Its localization error ranges between 10 and 30 cm, outperforming Bluetooth- or Wi-Fi-based distance measurement. The sensor data serve as input for the back-end positioning algorithm. For the real-time transmission of distance data, the helmet has sensing and localization capabilities. The helmet incorporates UWB distance sensors, wireless communication modules, voice broadcasting units, and an MCU. The overall helmet architecture is shown in Fig. 1, including four functional layers and their interactions.

2.1.2 Communication and data transmission layer

This layer transmits sensor data and other data from the sensing layer to the cloud management system. It consists of three functional units.

- The MCU serves as the central controller of the safety helmet. It collects raw sensor data, formats and performs preliminary analysis, and continuously monitors device status, such as sensor malfunction or low battery. The MCU organizes sensor data from the UWB module and manages voice playback functions. For example, when a worker powers on the helmet, the MCU is activated, establishes a network connection, and begins real-time distance monitoring. In addition, it coordinates communication with the cloud system and triggers local alerts when abnormal conditions are detected.
- The broadcasting unit provides voice alerts and response channels, triggered either by the MCU or the cloud management system (Fig. 2). Pre-recorded audio files are encoded and stored in the microcontroller for playback when alerts are activated.

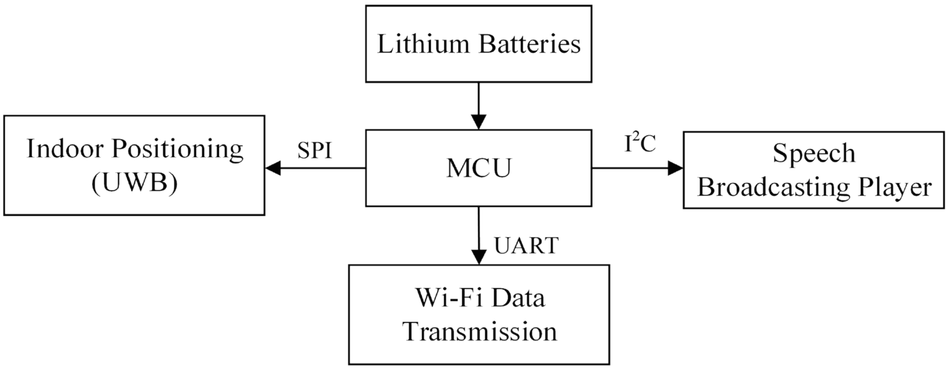

(a)

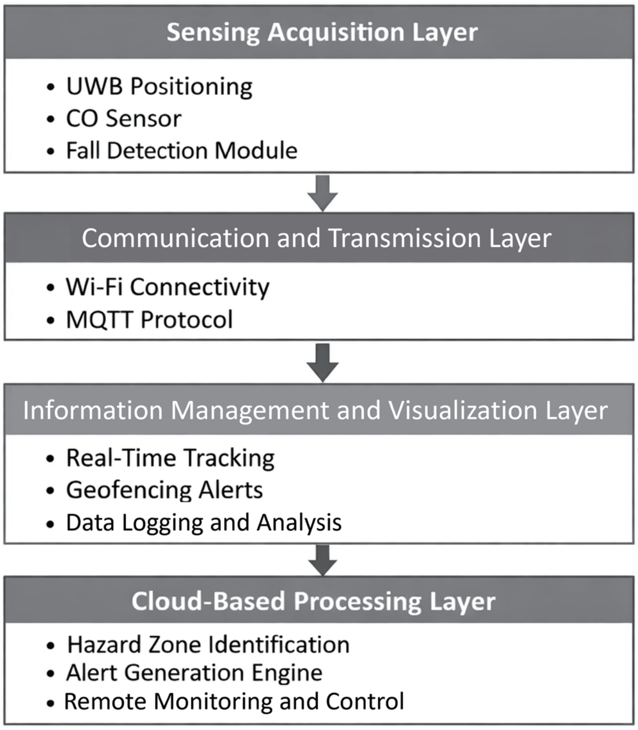

(b)

Fig. 1. Hardware configuration and system architecture of smart safety helmet developed in this study: (a) internal device layout and (b) layered system architecture (SPI: serial peripheral interface, I2C: inter-integrated circuit, UART: universal asynchronous receiver/transmitter, CO: carbon monoxide, and MQTT: message queuing telemetry transport).

- Passive reception: When the helmet receives broadcast or individual notifications from the server through MQTT, the unit parses the payload code and plays the corresponding audio alert (Table 1).
- Active broadcast: When the MCU detects abnormal conditions, a button is pressed, or a device malfunction occurs, the unit sends alerts to the cloud system through MQTT while simultaneously triggering local voice playback to notify the wearer.

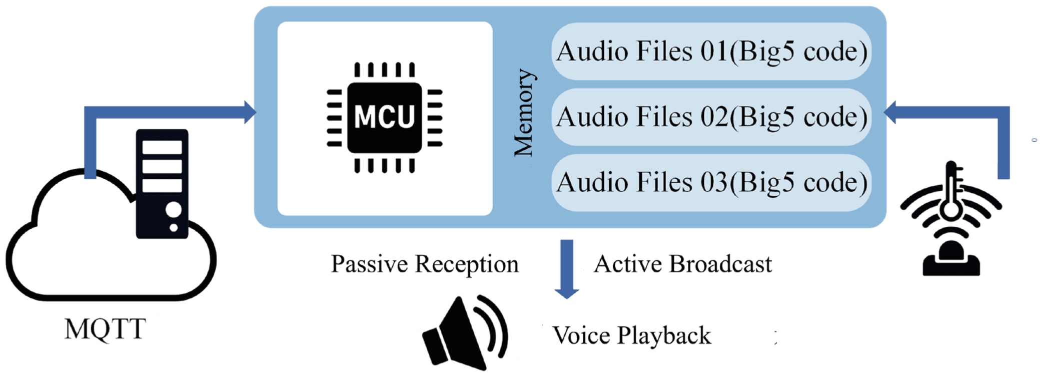

Fig. 2. (Color online) Broadcasting unit.

Table 1
Broadcasted messages.

Code	Abnormal condition/state category	Description	Voice message
0	Normal operational state	Start work	Status safe, continue working!
1	Normal operational state	End/break	Break time has started!
2	Site-safety anomaly (critical)	Evacuation notice	Please evacuate immediately to a safe area!
3	Systemic anomaly (hardware)	Low battery/sensor error	Warning: Device malfunction or low battery!
4	Site-safety anomaly (manual)	Emergency button pressed	Emergency signal sent! Help is on the way.
0	Normal spatial state	In safe zone	No voice broadcast
1	Site-safety anomaly (spatial)	In hazardous area	Do not approach this hazardous area!
2	Site-safety anomaly (proximity)	Near heavy machinery	Do not approach this hazardous area!

- The wireless transmission unit transmits sensor data and device status processed by the MCU back to the cloud management system using the MQTT protocol. Continuous communication ensures the frequent transmission of sensing data, localization information, and abnormal alerts. MQTT was used for its real-time capability, reliability, low latency, low resource consumption, and bidirectional messaging support.

2.1.3 Information management and visualization layer

This layer provides the interface that interacts with the system and performs real-time data visualization, personnel management, and abnormal event notifications. It consists of the following modules:

- a device management module that displays a list of all sensing devices and base stations, enabling monitoring and configuration;
- a personnel management module that manages worker profiles and access rights, allowing supervisors to query and track personnel status and localization records;
- an area management module that supports base station deployment, geofencing, and auxiliary distance measurement; by integrating engineering drawings with site coordinates, this module ensures that localization data correspond to real-world positions and issues alerts when workers enter or exit hazardous zones;

- a display module that visualizes worker positions and statuses on the front-end interface, along with immediate alert notifications.

2.1.4 Cloud-based data processing layer

As the core of the safety monitoring system, this layer receives sensing data through wireless communication and executes algorithms for localization, anomaly detection, and alerting. It consists of the following four modules:

- a communication module that facilitates communication with the front-end management layer through WebSocket and representational state transfer application programming interfaces, and with the communication transmission layer through MQTT;
- a data storage module that stores localization results, personnel status, and alert records in a non-relational database (MongoDB, a document-oriented database designed for high-volume data storage), supporting high-frequency data writing and flexible queries;
- an alert logic module that is responsible for anomaly detection and the execution of real-time alert mechanisms; the system distinguishes (1) systemic anomalies, including sensor hardware malfunctions, critical lithium battery depletion, high-confidence localization geometry failures (non-intersecting distance circles or abnormal anchor radii), and network packet timeouts, and (2) site-safety anomalies, including unauthorized worker entry into static geofenced danger zones, hazardous proximity to dynamic heavy machinery perimeters, and the manual activation of the emergency distress button; notifications are transmitted to the front-end management interface or directly to wearable devices through the MQTT protocol, ensuring immediate and reliable dissemination of safety alerts;
- a localization module that accurately tracks worker positions in real time using indoor and short-range localization technologies.

In workplaces, real-world environments introduce interference factors such as multipath effects, obstructions, and signal attenuation (Fig. 3). Therefore, common and atypical distance intersection conditions are analyzed in potential geometric scenarios (Fig. 4). There are unique intersections, pairwise intersections, multiple overlaps, tangency, or non-intersections of signals in the workplace. These interferences affect the existence, stability, and credibility of localization solutions. Abnormal cases, such as three circles with no intersection or inconsistent radii, indicate measurement inaccuracies, base station errors, or poor communication quality.

2.2 Enhanced trilateration method

To address signal interference, we used a multi-algorithm weighted fusion positioning algorithm (enhanced trilateration method) by integrating enhanced trilateration,[11] enhanced nonlinear least squares (ENLS),[12,13] and multi-circle overlap positioning. Dynamic weights are assigned to sensor data based on each algorithm's credibility under varying distance conditions, and weighted results are integrated to obtain the final position coordinates. The integrated algorithm ensures the accuracy of least-squares methods, the adaptability of multi-circle overlapping, and the robustness of trilateration corrections. The integrated algorithm adjusts

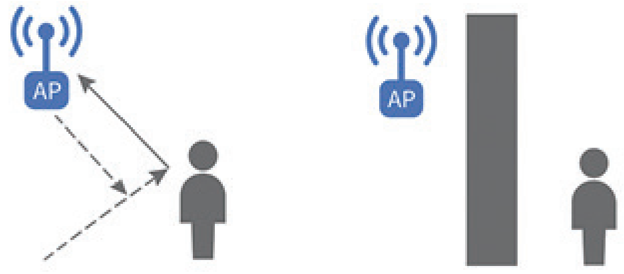

(a) (b) (c)

Fig. 3. (Color online) Bottlenecks encountered in positioning technology: (a) multipath effect, (b) obstruction, and (c) wireless signal attenuation.

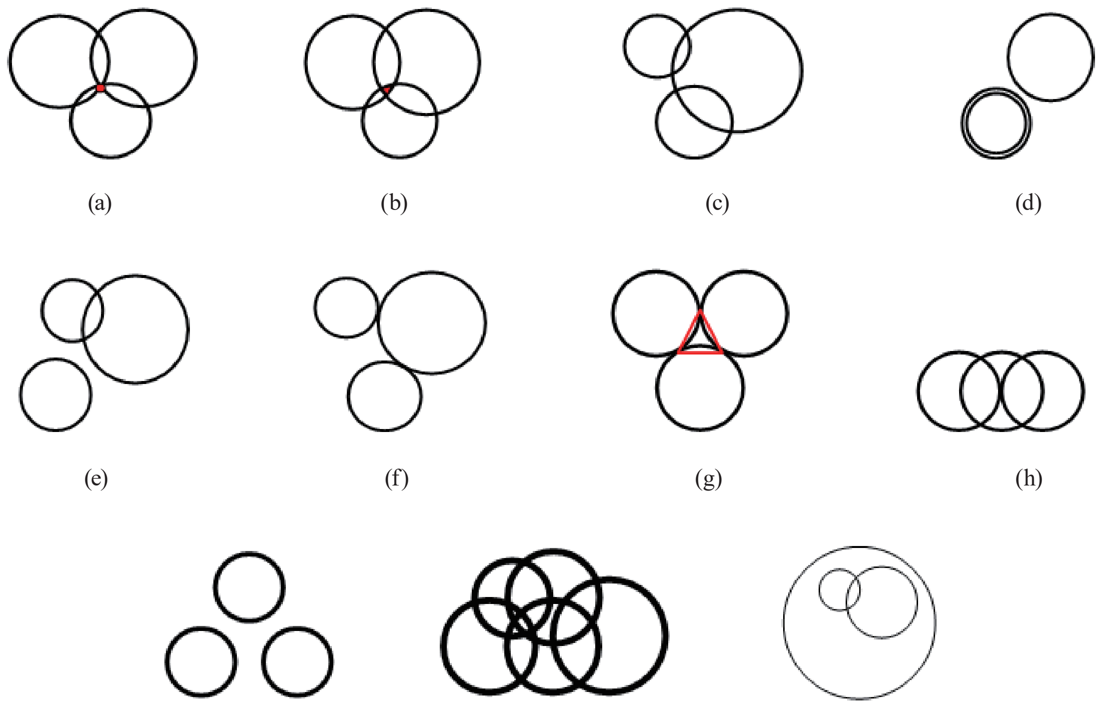

(a) (b) (c) (d)

(e) (f) (g) (h)

(i) (j) (k)

Fig. 4. (Color online) Possible situations in three-point positioning [(a) three circles intersect at a single point, (b) three circles intersect (common overlap region), (c) two circles intersect within one circle, (d) two circles overlap, third circle has no intersection, (e) two circles intersect, one circle has no overlap, (f) two circles tangent within one circle, (g) three circles tangent to each other, (h) three circles aligned in parallel (near-collinear anchors), (i) three circles with no intersection, (j) multiple circles intersect (multi-overlap region), and (k) one circle has abnormal radius (measurement error).

weights on the basis of a confidence level and historical trajectory data to yield reliable localization results (Fig. 5).

In conventional trilateration, multiple geometric configurations produce large errors. For example, when three APs are collinear or when the triangle formed by the APs has a minimum

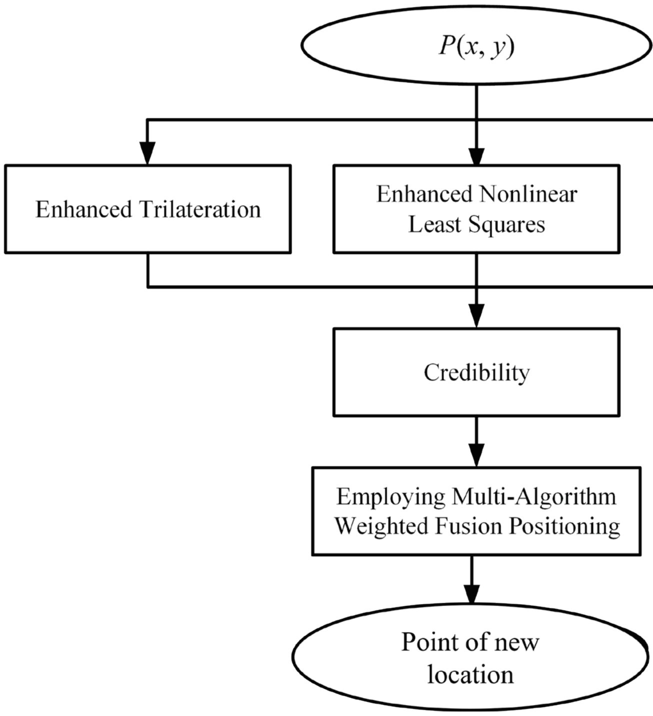

Fig. 5. Workflow of integrated algorithm.

interior angle θ_{min}, triangulation cannot be a valid solution. To overcome these limitations, we used an enhanced trilateration method. This method retains the geometry of three-point coordinate estimation for the following improvements:

- angle filtering by excluding configurations where θ_{min} is below a threshold;
- group combination filtering to select valid AP combinations to improve robustness;
- credibility evaluation to assign confidence scores to candidate solutions based on geometric stability;
- directional adjustment to align estimated positions with historical trajectory data to reduce sudden deviations.

These enhancements (Table 2) enable stable distance estimation even in noisy, interference-prone construction environments.

For such improvements, the mathematical framework for the enhanced trilateration method is established by refining the geometric relationships between anchors and targets as follows. When three APs are located at the coordinates (x_i,y_i) ($i = 1, 2, \ldots, 3$), with measured distances d_i to the target point (x, y), the basic trilateration equations are expressed as

$$(x - x_i)^2 + (y - y_i)^2 = d_i^2,\ i = 1,2,3\,. \tag{1}$$

Table 2
Improvements in enhanced trilateration method used in this study.

Data	Trilateration method	Enhanced trilateration method
Input data	Three anchor positions and distances	Same input: three anchors and distances
Computation principle	Geometric method to avoid intersections	Geometric method with orthogonal basis, using projection vectors
Error handling	No error handling, solution returned directly	Incorporating effect-based weighting to adjust distance errors
Angle check	No angle check	Adding minimum angle filtering and excluding triangles with small angles
Multiple combinations	Fixed selection of one set of three anchors	Iterating all combinations (${}_nC_3$) of three anchors, evaluating concentration, and selecting credible sets
Result selection	No weighting	Scoring all candidate results using directional vector similarity and displacement penalty and selecting best combination

By subtracting pairs of equations and quadratic terms, linear relationships are presented as

$$2\left(x_j - x_i\right)x + 2\left(y_j - y_i\right)y = d_i^2 - d_j^2 + x_j^2 - x_i^2 + y_j^2 - y_i^2 \tag{2}$$

for $i \neq j$. By solving these linear equations, candidate coordinates are obtained. In the enhanced trilateration method, the following refinements are applied:

(1) angle constraint: if, the solution is discarded to avoid instability;

(2) credibility weighting: each candidate solution is assigned a credibility score w_i based on geometric stability and signal quality;

(3) directional adjustment: historical trajectory vector is used to refine the solution

$$(x, y)_{enhanced} = \left(x, y\right) + \alpha \cdot \vec{v}_{t-1}, \tag{3}$$

where α is a correction factor proportional to credibility.

The enhanced trilateration method improves the robustness of UWB sensor-based localization in multipath-heavy construction sites. Credibility evaluation and trajectory adjustment results demonstrate how sensor data can be weighted to improve accuracy. This method directly contributes to sensor data fusion, ensuring reliable positioning in complex industrial environments.

2.3 Enhanced nonlinear least squares

NLS is a widely used localization method to estimate target positions by minimizing an error function on the principle of statistical least-squares optimization and to achieve robust results even in non-ideal environments.[12,13] In using NLS, measurement errors are assumed to be independent, normally distributed, and equally weighted across all sensing points. The estimation process begins with an arbitrary initial value and iteratively refines the solution using

Newton's method or simplified gradient descent until convergence to a local minimum of the loss function. However, in the workplace, conventional NLS faces challenges that degrade accuracy and convergence performance as follows.

- Accumulated measurement errors: Multiple distance measurements often contain bias. If one or more measurements deviate significantly, the overall squared loss function may diverge from the true solution.
- Poor geometric structure: When anchor points are collinear or overly concentrated, the solution space becomes degenerate, leading to unstable convergence directions.
- Outlier interference: In crowded or abnormal scenarios, distance measurements might exhibit extreme deviations, resulting in unreliable estimates.

To address these limitations, we enhanced the ENLS method for the following improvements (Table 3):

- optimized initial value strategy: selecting starting points based on geometric heuristics or historical trajectory data to avoid poor convergence;
- dynamic residual filtering: identifying and excluding outlier measurements during iterations to reduce bias;
- convergence credibility assessment: introducing a confidence evaluation mechanism to determine whether the solution is reliable.
- directional vector consistency check: comparing estimated trajectory vectors with historical movement patterns to ensure directional stability;
- multi-level credibility output: providing layered confidence scores for integration into the weighted fusion framework.

To implement these improvements, the conventional NLS is mathematically restructured to incorporate dynamic filtering and credibility weighting. The formulation of this enhanced optimization process is as follows. Let the target position be (x, y) and the measured distance to anchor i be d_i. The error function is defined as

$$E(x,y)=\sum_{i=1}^{n}\left(\sqrt{(x-x_i)^2+(y-y_i)^2}\mid d_i\right)^2. \tag{4}$$

Table 3
Improvements in NLS method.

Evaluation aspect	NLS	ENLS
Initial position setting	Using average of measurement points or fixed initial constant	Using results from other localization methods or historical positions as hint points
Error model	All points treated with equal weight in residuals	Analyzing residual distribution at each iteration and excluding outliers beyond ±2 standard deviations
Convergence criterion	Terminating based on allowable error threshold	Considering convergence speed and total error, and adjusting credibility
Vector information	Not utilized	Incorporating movement vector comparison as a basis for credibility adjustment
Credibility design	None	Reflecting stability and reliability with multi-level credibility

Conventional NLS minimizes $E(x,y)$ through iterative optimization. In ENLS, the following refinements are applied:

- Residual filtering: At each iteration, residuals r_i are computed as

$$r_i = \sqrt{(x-x_i)^2 + (y-y_i)^2} - d_i \,. \tag{5}$$

Residuals exceeding a dynamic threshold τ are excluded from the next iteration.

- Credibility weighting: Each residual is assigned a weight w_i on the basis of its consistency with historical trajectory and geometric stability.

$$E_{\text{ENLS}}(x,y) = \sum_{i=1}^{n} w_i \cdot r_i^2 \tag{6}$$

- Directional adjustment: The solution is refined using the historical trajectory vector $\vec{v}_{t-1}$.

$$(x,y)_{\text{ENLS}} = (x,y) + \beta \cdot \vec{v}_{t-1} \tag{7}$$

Here, β is a correction factor proportional to credibility.

When the system receives n data points from anchors, with known positions $P(x_i, y_i)$ and measured distances r_i to the helmet wearer, the following NLS loss function is defined as the minimization objective:

$$L_{min} = \sum_{i=1}^{n} \left(\sqrt{(x-x_i)^2 + (y-y_i)^2} - r_i \right)^2 . \tag{8}$$

Since this is an NLS problem and the square root term prevents obtaining a direct linear solution, numerical approximation is required through iterative updates. The iteration begins from an initial value obtained from the overlap method or trilateration. The average of measurement points is used as the initial point $P(x_0, y_0)$. This method improves convergence efficiency and reduces bias. Each participating anchor contributes partial derivatives with respect to $P(x,y)$, forming the update direction using the following correction equation:

$$x_{k+1} = x_k - \alpha \cdot \sum_i \frac{e_i (x_k - x_i)}{\sqrt{(x_k - x_i)^2 + (y_k - y_i)^2}} , \tag{9}$$

$$y_{k+1} = y_k - \alpha \cdot \sum_i \frac{e_i (y_k - y_i)}{\sqrt{(x_k - x_i)^2 + (y_k - y_i)^2}} , \tag{10}$$

Here, α is the learning rate, preset to 0.1, which controls the correction step size and prevents oscillation. Convergence is established when the magnitude of two consecutive updates falls below the tolerance threshold (e_i) or when the predefined maximum iteration limit is reached. To quantify the stability of each localization result, the total squared error is calculated as

$$E = \sum_i e_i^2 \, . \tag{11}$$

With the iteration count, a credibility level according to the conditions is defined as follows (Table 4). When localization has prior position information $P\left(x_{last}, y_{last}\right)$, its direction vector $\vec{v}_{last}$ is computed and compared with the current estimated displacement vector $\vec{v}_{current}$ by calculating the cosine similarity cosθ. The similarity serves as a credibility adjustment factor. The correction equation is expressed as

$$Credibility_{adjusted} = Credibility_{base} \cdot \cos\theta \, , \tag{12}$$

$$Credibility = Base \times \max\left(0.1, \cos\theta\right),\ \cos\theta = \frac{\vec{v}_{current} \cdot \vec{v}_{last}}{\left\|\vec{v}_{current}\right\| \cdot \left\|\vec{v}_{last}\right\|} \, . \tag{13}$$

This method filters out high-confidence errors caused by abnormal vector generation. By adopting a direction-scoring strategy consistent with that used in the enhanced trilateration method, ENLS is used for coordinated multi-module decision-making. The ENLS method provides continuous and consistent localization solutions when sufficient observation points and reasonable initial conditions are available. Because the effect of each measurement is quantitatively processed, no single point dominates the overall result, thereby improving fault tolerance. However, ENLS' convergence speed is constrained by initial conditions and residual characteristics. When data quality is poor, the algorithm fails to converge and yields biased solutions. These limitations highlight the importance of integrating ENLS into a multi-algorithm weighted fusion framework, where its strengths in robustness and fault tolerance enable the geometric precision of the enhanced trilateration method.

Table 4
Credibility criteria for ENLS localization.

Stability level	Error/iteration	Credibility level
High stability	Iteration count < 20 and $e < 10^5$	0.8
Moderate stability	Iteration count 20–40 or $e < 5 \times 10^5$	0.5
Low stability	Iteration count > 80 or $e > 10^6$	0.2

2.4 Multi-circle overlap positioning method

Even with the enhanced trilateration and ENLS methods, distance measurements from anchor points might suffer from nonlinear bias, uneven distribution, and directional obstructions. Under such conditions, single-point estimation results are distorted by extreme measurement errors. To address this issue, we designed a multi-circle overlap positioning method, which adopts a spatial coverage approach. In the method, each distance measurement is treated as a sensing circle, with the anchor point coordinates (x_i, y_i) as the center and the measured distance r_i as the radius. When the system receives n measurements, n circles are drawn. If measurements are error-free, the intersection of these circles converges to a single point (Fig. 6). However, measurement errors and sensor bias make the intersection region irregular.

Therefore, we used a method to estimate the target position $P(x, y)$ as the geometric centroid of the overlapping region, while overlap density serves as the credibility metric. The workflow of the multi-circle overlap positioning method is as follows.

(1) Candidate point sampling: A grid of candidate points is generated across the field with a predefined resolution. For each grid point, distances to all anchors are calculated.

(2) Overlap scoring mechanism: If the distance between a candidate point and anchor i satisfies $|d_i - r_i| < \delta$, the point is considered within the sensing circle of anchor i, and its overlap score is incremented.

(3) Maximum overlap region search: Candidate points with overlap scores greater than or equal to m (in this study, at least two-circle overlap) are grouped to form the overlap region.

(4) Position estimation: The final estimated position $P(x, y)$ is computed as the average coordinates of all candidate points within the overlap region.

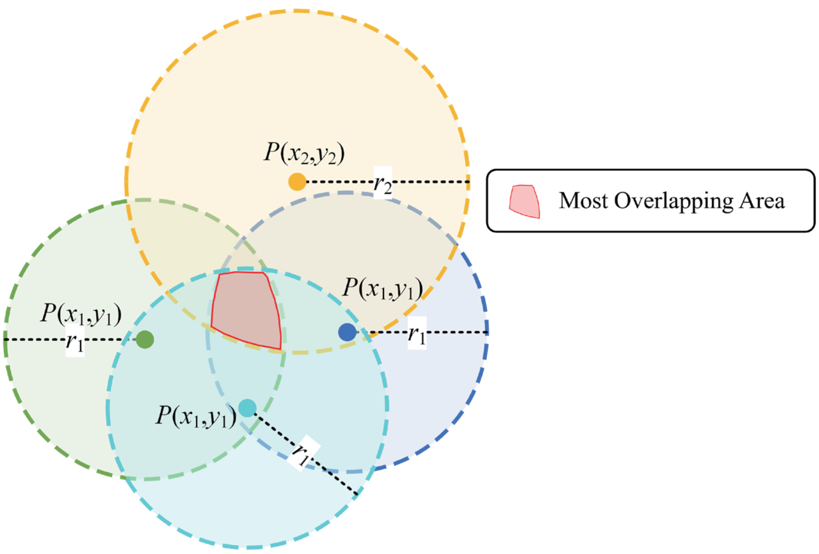

Fig. 6. (Color online) Intersections of sensing circles and most overlapping area.

$$P(x,y) = \frac{1}{k}\sum_{j=1}^{k}(x_j, y_j) \tag{14}$$

Here, k is the number of candidate points in the overlap region.

(5) Credibility evaluation: A credibility score is assigned on the basis of the maximum overlap count, overlap density, and dispersion of candidate points. This score is then used in the fusion framework.

The multi-circle overlap method does not rely on initial values or gradient information. Therefore, it is appropriate for scenarios with poor anchor distribution, such as two anchors too close, distorted geometry, large measurement errors, or concentrated bias in certain anchors. By focusing on spatial overlap rather than strict error minimization, this method enhances fault tolerance and stability in noisy environments. To describe the reliability of the current localization estimate, the system computes the standard deviation σ and the maximum overlap count from the point set. On the basis of these values, a corresponding credibility score is assigned according to the conditions shown in Table 5.

2.5 Fusion and final localization

After obtaining individual localization results and credibility scores from the enhanced trilateration, ENLS, and multi-circle overlap positioning methods, weighted data fusion is conducted. Weighted data fusion aims to synthesize the outputs of different algorithms into a single final localization result, taking into account spatial conditions, error characteristics, and historical trajectory information. Before performing weighted data fusion, the characteristics and applicability of each method must be analyzed in different scenarios. Although all the methods use distance measurements as their input data, their processing methods, stability, tolerance to errors, and computational burdens differ. These differences offer the basis for weight assignment and reliability evaluation in the fusion process. The fusion mechanism operates as follows.

(1) Output collection: Each algorithm produces an estimated position $P_i(x,y)$ and a credibility score C_i.

(2) Dynamic weight assignment: Weights w_i are assigned to each algorithm on the basis of its credibility score and environmental suitability.

Table 5
Evaluation criteria for multi-circle overlap method.

Condition	Credibility level
$M \geq 5$ and $\sigma < 3$	0.8
$M \geq 4$ and $3 \leq \sigma < 6$	0.6
$M < 3$ or $\sigma \geq 6$	0.3

$$w_i = \frac{C_i}{\sum_{j=1}^{3} C_j} \tag{15}$$

(3) Localization: The final estimated position $P(x,y)$ is computed as

$$P(x,y) = \sum_{i=1}^{3} w_i \cdot P_i(x,y). \tag{16}$$

(4) Reliability assessment: The fused result is validated by comparing its directional consistency with historical trajectory vectors and by assessing overlap density in candidate regions.

The strengths and weaknesses of the three algorithms are summarized as presented in Table 6. The methods ensure representative and relatively credible localization outputs even under extreme conditions, avoiding situations where no result is produced or where errors are concentrated in a single source. The methods used in this study operate independently but complement and reinforce one another in terms of data quality, spatial geometry, and historical trajectory consistency. As a result, the localization outcome has continuity, stability, and environmental adaptability, establishing a reliable methodology for subsequent event reporting and smart occupational safety applications. This integrated method enhances the robustness of sensor-based positioning and ensures that the monitoring platform can deliver accurate, real-time information essential for emergency response and workplace safety management.

Table 6
Comparison of three localization algorithms.

Evaluation aspect	Enhanced trilateration method	ENLS	Multi circle overlap method
Computational complexity	Low (direct geometric calculation)	Medium (requires iterative optimization)	High (spatial sampling and overlap statistics)
Error sensitivity	High	Medium	Low
Dependence on initial value	None	Yes	None
Anchor structure requirement	High (requires stable three-anchor geometry)	Medium (≥3 anchors, stable distribution)	Low (only two anchors sufficient; effective in corridors or elongated areas)
Result stability	Medium	Medium	Medium to High
Credibility basis	Dispersion (standard deviation) + direction vectors	Residual statistics + movement vector similarity	Overlap count M + dispersion σ + directional consistency
Suitable scenarios	Stable three-point geometry; uniform error distribution	Sufficient anchor points; reliable movement vector reference	Severe occlusion; asymmetric errors; abnormal data distribution

2.6 Experiment

To evaluate the localization precision and reliability of the smart safety system, structured data were collected within a multi-level concrete atrium designed to mimic an unfinished building framework. The test venue was selected for its open structure, moderate spaciousness, and controllability, making it appropriate for the initial verification of localization accuracy and algorithmic convergence stability (Fig. 7). The test venue features a total floor area of 450 m^2 (18 × 25 m^2) with structural columns. The experiment was conducted by 120 participants recruited from the university digital media arts and vocational engineering programs. A total of 150 independent trials were performed along pre-mapped test paths. As indicated by the blue markers in Fig. 7(b), eight localized UWB APs were installed. These sensors comprised fixed-position MaUWB-DW3000 transceiver nodes that continuously broadcast and receive sub-nanosecond pulses to compute raw distance vectors via precise bidirectional time-of-flight ranging when queried by an active helmet tag. During the test, coordinates were recorded at a sampling rate of 10 Hz, yielding more than 15000 distinct spatial data points for accuracy analysis. Before testing, laser rangefinders were used to obtain reference distances for calibration.

3. Results and Discussion

3.1 Smart safety helmet

We fabricated a smart safety helmet integrating an MCU, a UWB module, and a broadcasting unit (Fig. 8). The localization module employed was the MaUWB-DW3000 (Makerfabs, China), a compact UWB transceiver based on the Qorvo DW3000 integrated circuit. This module is widely adopted in high-precision indoor positioning systems and supports bidirectional communication using time-of-flight algorithms for distance estimation. For voice playback, the SD178BMI module was implemented. To ensure user comfort and avoid interference with wearability, the circuit board was installed in the hollow top region of the helmet.

Operating on a channel bandwidth of 499.2 MHz centered at 6.489 GHz, the DW3000 transceiver determines range through precision ToF estimation and can resolve picosecond pulse arrival times at the physical layer. To complement its spatial ranging capability, a low-power multi-axis micro-electromechanical system (MEMS)-based inertial measurement unit (IMU) was integrated. These auxiliary sensors continuously monitor linear acceleration and angular velocity along three orthogonal axes, providing localized posture telemetry. Sudden decelerations detected by IMU are correlated with positional data to identify fall events, enabling the helmet to deliver immediate safety alerts.

In the safety monitoring system, the data are collected and transmitted to the localization computation unit, whereas the cloud platform receives distance data between the helmet and the server. The system executes the enhanced trilateration, ENLS, and multi-circle overlap positioning methods, followed by weighted fusion to estimate worker positions.

(a)

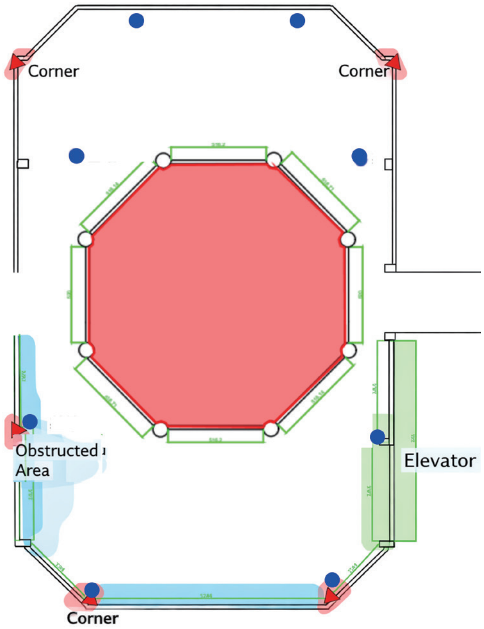

(b)

Fig. 7. (Color online) Sensor implementation in campus building: (a) campus building (UWB AP circuit board with MCU and connectors in red boxes) and (b) sensor installation location (blue circle: sensor location).

3.2 Test result

The test was conducted in a full loop around the atrium, with the participants wearing the sensing helmet and following a pre-planned path. The trajectory incorporated multiple corners, obstructed areas, and elevator zones to replicate industrial conditions characterized by poor

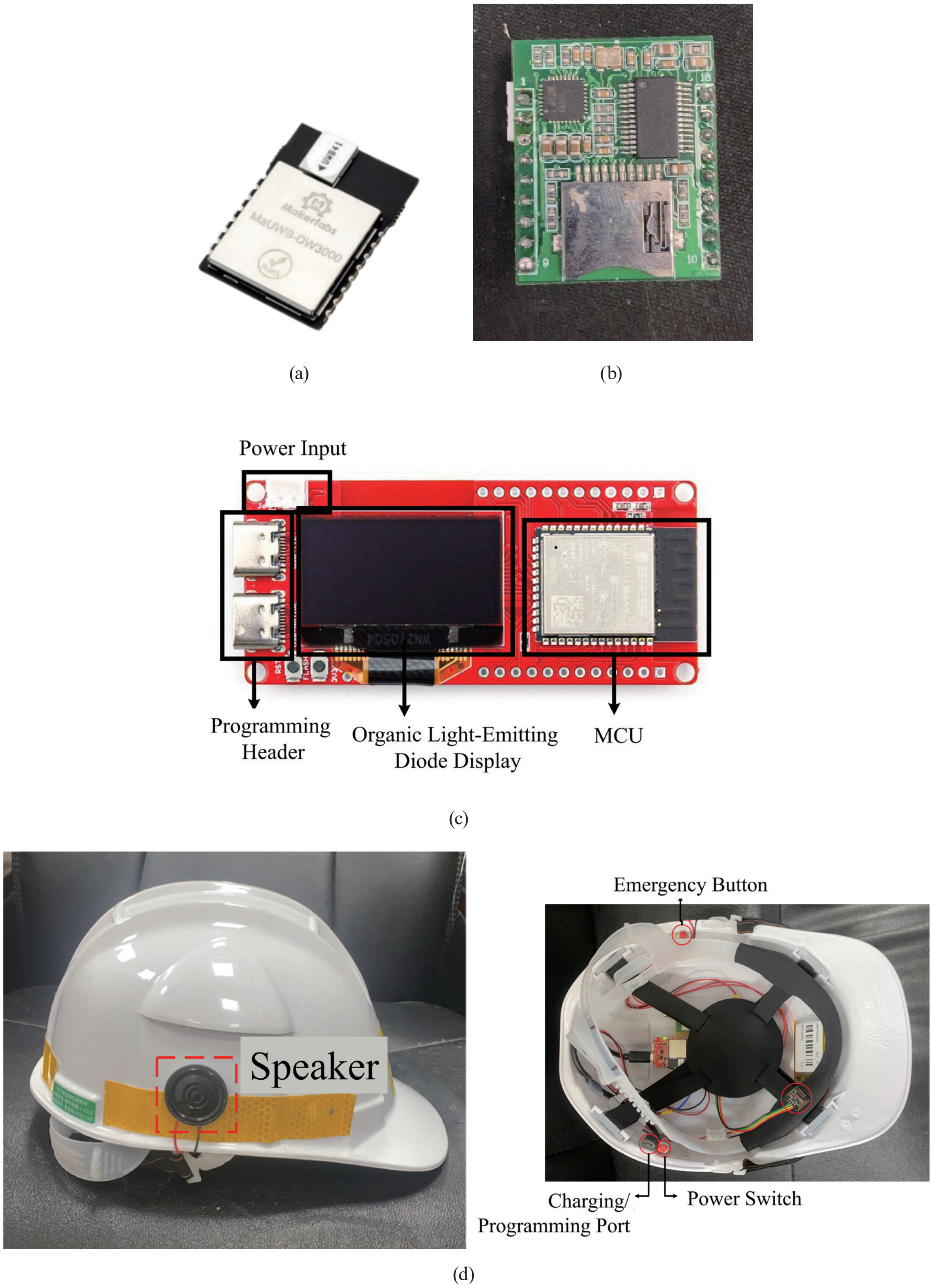

Fig. 8. (Color online) Main components of smart safety helmet and its appearance: (a) MaUWB-DW3000, (b) SD178BMI voice module, (c) MaUWB_ESP32S3 UWB module development board, and (d) safety helmet (external and internal views).

localization geometry [Fig. 9(a)]. When applying the enhanced trilateration method, scattered coordinate points appeared at corner regions, particularly in the upper-right and lower-left zones [Fig. 9(b)]. This instability stems from small anchor angles, which amplify the geometric dilution of precision and produce discontinuous results, validating the limitations summarized in Table 7.

The ENLS method generated smoother trajectories than trilateration but exhibited localized drift at corners and obstructed areas [Fig. 9(c)]. At the upper-left return corner, the estimated path showed unrealistic inward bends, a consequence of poor initial conditions and large anchor measurement errors. These errors caused the iterative optimization process to converge toward local minima, underscoring ENLS's dependence on accurate initialization. The multi-circle overlap method achieved superior continuity and fault tolerance [Fig. 9(d)], particularly in narrow corridors where three-anchor geometry collapses. By computing the centroid of overlapping circles, this method demonstrated resilience under obstruction and uneven anchor distribution. However, when overlap regions were small, centroid estimates deviated inward, as observed along the left side of the trajectory.

By implementing the dynamic weighted fusion rules, the system successfully balanced the strengths and weaknesses of each constituent algorithm in real time according to their situational credibility scores. As shown in Fig. 9(e), the integrated trajectory closely matched the true reference path, maintaining smoothness and continuity across varying environmental conditions.

In regions with linear anchor distributions and severe occlusion, such as the upper and lower-left corners, the system detected drops in trilateration and ENLS credibility metrics due to high residuals and geometric dispersion. The fusion architecture dynamically reallocated weights toward the multi-circle overlap method. Conversely, in open corridors with stable geometry, weights shifted back to the low-overhead trilateration method to conserve processing bandwidth.

In 150 logged trials, localization errors were aggregated to evaluate performance under severe multipath and non-line-of-sight conditions. The cumulative distribution function of tracking errors confirmed that the fused model maintained submeter accuracy for all participants, even under dynamic body shielding effects. The results of a multivariate analysis of variance (MANOVA) showed that localization precision improvements were statistically significant against variations in participant morphology ($p > 0.05$), walking velocity, and structural reflection profiles.

By combining geometric convergence, optimization residuals, and historical trajectory vectors, the integrated platform effectively filtered out spatial anomalies and preserved tracking continuity. These results establish a reliable, field-validated sensing foundation for real-time hazard geofencing and smart occupational safety applications.

3.3 System application

The barriers to deploying smart sensor networks on large construction sites (larger than 10000 m^2) are the cost of wiring and the computational bottlenecks associated with scaling. The system developed in this study addresses these challenges through an unanchored, decentralized

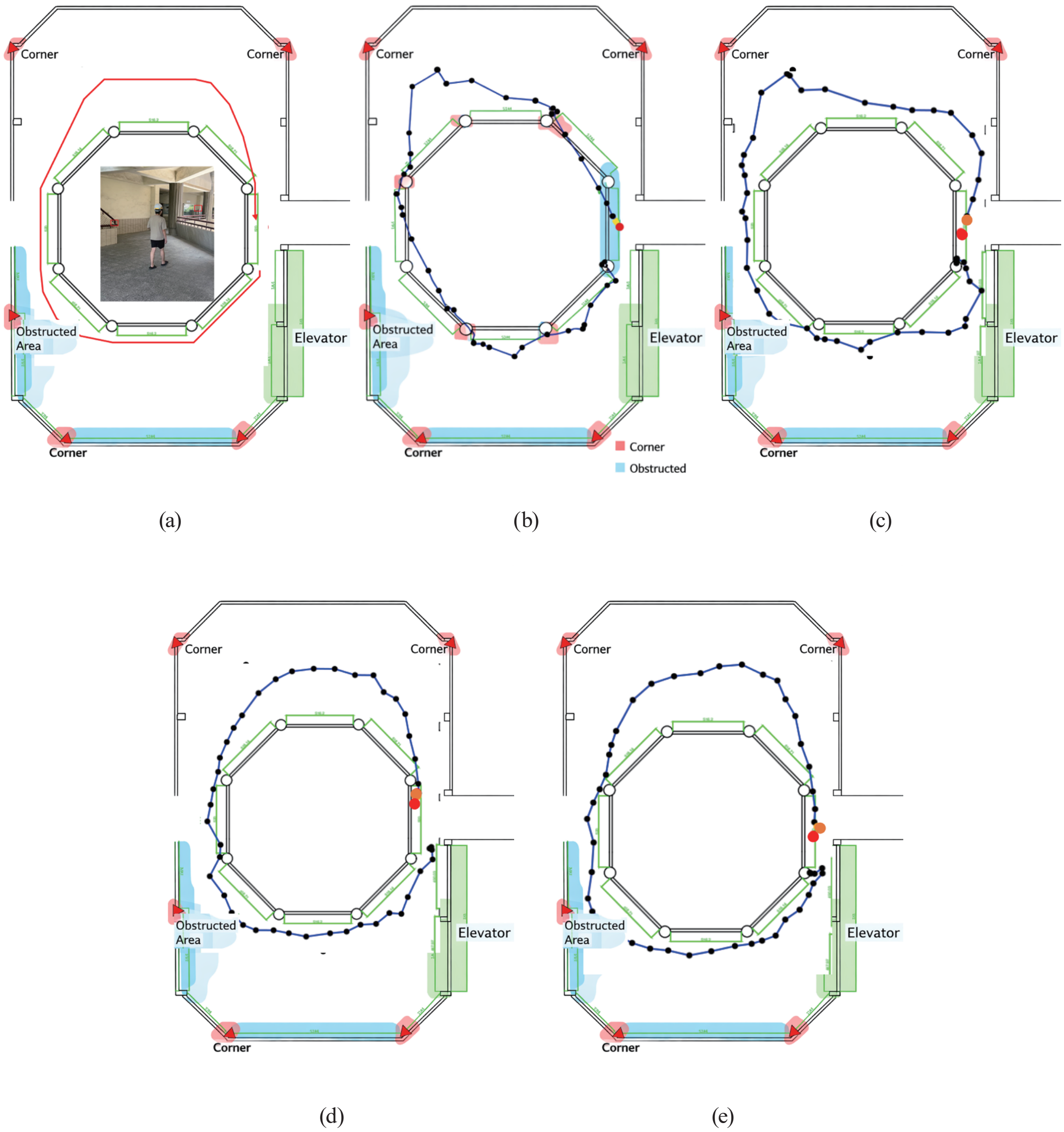

Fig. 9. (Color online) Comparison of individual localization results among different methods (red line represents preplanned walking path followed by participant for reference calibration, orange dot represents computed coordinate position calculated using algorithms at a sampling rate of 10 Hz, and blue line and circle represent fixed coordinates of UWB APs distributed asymmetrically across the test floor): (a) path for testing in testing venue, (b) individual localization using enhanced trilateration method, (c) individual localization using ENLS, (d) individual localization using multi-circle overlap method, and (e) individual localization using integrated method.

communication architecture. Because the safety helmet functions as the processing device to collect raw UWB data and transmit the compressed coordinate packets through WiFi or cellular networks to the cloud server, the eight APs do not need wired data backbones or local internet connections. This design eliminates the need for costly cabling across expansive and nonstatic structural environments.

For cost-effective scalability, a cellular spatial grid layout can be employed. As workers move across large zones, the helmet automatically performs localized handovers, communicating with the three or four nearest line-of-sight APs within its immediate radiofrequency cell. This grouping constrains the computational complexity of enhanced trilateration and ENLS matrix resolutions, preventing cloud processing delays as more devices are included in the network. Combined with DW3000 transceiver modules, this cellular grid architecture enables safety managers to expand tracking coverage across large projects with minimal hardware investment, offering a practical and highly scalable solution for industrial safety management.(14)

Such capability can solve the impossibility of installing sensor networks at regular or symmetrical spatial intervals due to irregular structural designs and physical obstructions in construction sites. The multi-algorithm matrix treats anchor locations as arbitrary, non-uniform coordinate parameters stored in the cloud database. When irregular spacing causes localized geometric degradation, such as a dense cluster of APs in an open zone followed by a sparse, asymmetric distribution in a narrow corridor, the smart safety system's algorithmic diversity serves as a mathematical buffer.(15) For instance, when asymmetric geometry impairs the initial values required for standard ENLS convergence, the multi-circle overlap module continues to output robust coordinates on the basis of density intersections rather than rigid angular symmetry. By continuously evaluating situational credibility metrics derived from geometric shapes and measurement residuals, the weighted fusion layer smoothly tracks the user across irregular sensor configurations without requiring changes to the underlying physical layout.

The scale-up of the smart safety system in large areas requires dedicated cloud-connected gateways on every floor, which is economically redundant. Because the smart safety helmet functions as an autonomous data collection agent, compressed coordinate packets can be transmitted on sub-GHz or cellular networks, bypassing reinforced concrete slabs and reaching centralized gateways positioned several floors apart. Nevertheless, maintaining a localized network of fixed UWB APs on each floor is essential, given the severe attenuation of 6.5 GHz radio pulses through reinforced concrete. Furthermore, symmetrical floor layouts introduce the risk of vertical ambiguity, where a tag may inadvertently range with anchors located directly above or below on adjacent floors. To address this limitation, a high-resolution barometric altimeter sensor must be integrated into the helmet. By fusing relative atmospheric pressure data with localized AP identification codes, the cloud processing layer can execute initial data filtering.(16) This procedure enhances trilateration and multi-circle overlap algorithms, establishing a true three-dimensional workplace safety framework.

3.4 Limitations and further development

In this study, we mainly evaluated the smart safety helmet by measuring how accurately its fused UWB tracking algorithm performed under difficult signal conditions. The helmet is not just a location tracker but a multi-hazard safety device. Its cost-effectiveness comes from combining functions into one platform. Instead of relying on separate, fragile gas or physiological sensors, the helmet collects high-frequency location data for cloud-based geofencing. In the performance evaluation, when a worker approached mapped danger zones, such as floor openings, edges, or areas with heavy machinery, the cloud system sent a warning through MQTT. The helmet's built-in speaker converted this into a clear voice alert, audible right away to the worker. This wearable system replaces multiple devices, such as tracking tags, hazard beacons, and manual alerts, proving its economic efficiency and value for risk reduction in high-hazard construction environments.

The geofencing mechanism of the developed safety helmet further enhances its adaptability for safety management. Because construction sites are dynamic and changing throughout different project phases, the helmet employs a cloud-managed geofencing architecture. Through a centralized management dashboard, safety coordinators can promptly redefine, expand, or relocate the coordinates of high-risk zones, such as temporary floor openings or blasting areas, as situations on site change. For heavy excavation machinery, a UWB anchor can be mounted on the vehicle. The cloud platform can compute the real-time relative distance vector between moving equipment and nearby workers, automatically activating the helmet's audio broadcasting unit when a predefined safety buffer is breached. The internal electronic modules for positioning, processing, and communication are included in the helmet. These modules are housed in a rugged, clip-on enclosure that attaches to personal protective equipment, such as full-body fall-arrest harnesses or high-visibility vests. By interfacing with limit switches or capacitive sensors integrated into harness buckles, equipment usage can also be monitored. For example, if a worker is detected near an elevated edge and the buckle sensor indicates an unfastened harness, an automated voice alert is issued to enforce compliance and prevent fall-related accidents.

Although commercially available UWB and MEMS components were used to validate a cloud-fused safety system in this study, advanced sensors and functional materials should be used in heavy industrial environments. Standard rigid Flame Retardant 4 Printed Circuit Boards impose physical design constraints and weights when embedded into protective helmets or wearable harnesses. To resolve this, flexible, stretchable polymeric substrates and screen-printed conductive silver inks can be used.[17] With organic, skin-like sensor patches, spatial tags and IMU circuits can be used to conform seamlessly to curved safety gear surfaces, increasing ergonomic comfort.

The multipath reflections and non-line-of-sight signal blocks caused by concrete walls and iron structures are bottlenecks for wireless tracking. To address those bottlenecks, passive, tunable electromagnetic metamaterial surfaces must be used.[18] Coated structural columns with engineered artificial materials can be used to optimize the indoor channel environment and smooth out the trilateration calculations since they absorb, refract, or reflect high-frequency (6.5 GHz) radio pulses. Continuous real-time sensor data streaming demands steady power. However, heavy lithium-ion batteries cause neck strain and present explosion hazards in high-temperature environments. With advanced solid-state polymer electrolyte batteries or flexible graphene-based supercapacitors,[19] thin, explosion-proof materials can be integrated directly into the polymer matrix of the helmet shell, achieving self-powered safety gear. Future smart safety systems can be developed by employing such advanced materials and technologies.

4. Conclusions

To address the challenges of occupational safety incidents in high-risk industrial environments that present insufficient real-time monitoring and unreliable localization mechanisms, a cloud-based workplace safety management system was developed in this study. The system integrates continuous positioning, dynamic spatial geofencing, and immediate voice broadcasting capabilities. It combines specialized wearable hardware with responsive IoT communication backplanes (MQTT and WebSocket) and adaptive multi-algorithm sensor data fusion. Through this integration, industrial supervisors can continuously assess personnel safety status and initiate instantaneous emergency responses when hazardous conditions arise.

A field test was conducted within a multi-level concrete atrium with an area of 450 m^2. The venue was designed to replicate the structural complexity of unfinished industrial sites, incorporating columns, elevator shafts, non-line-of-sight corridors, and asymmetric signal paths. One hundred and twenty participants completed 150 independent trials, generating over 15,000 high-frequency spatial coordinates at a sampling rate of 10 Hz. The results showed that the developed system effectively mitigated the physical-layer vulnerabilities inherent to individual baseline estimators. Whereas the enhanced trilateration and ENLS methods showed coordinate scattering, the geometric dilution of precision anomalies, and local-minimum convergence at 90° turns or structural boundaries, the developed fusion system maintained smooth and continuous tracking. The fused positioning model achieved submeter localization accuracy across all participants. The MANOVA result showed that these precision improvements were statistically significant against variations in participant morphology, walking velocity, and dynamic body-shielding attenuation.

The test result can be used to develop sensor deployment architecture beyond traditional single-source filtering approaches such as Kalman filters, which often fail under non-Gaussian noise conditions typical of obstructed industrial environments. By introducing a dynamic weight-allocation matrix derived from geometric interior angles, optimization residuals, and historical trajectory vectors, the system processed raw radio-frequency metrics under severe multipath interference. The developed system integrates multi-axis MEMS IMUs with high-frequency Qorvo DW3000 UWB transceivers in a compact configuration. This design enables the seamless interfacing of heterogeneous sensor data, including continuous spatial coordinates, physical posture vectors, and irregular distress signals with cloud-based analysis.

By introducing an unanchored deployment strategy, the developed system minimizes infrastructure requirements. The safety helmet functions as a main processing bridge, transmitting compressed coordinate data to the cloud server, whereas fixed APs operate without wired communication backbones. By organizing large construction zones into a cellular spatial grid layout, the system constrains local computational complexity and supports cost-effective scalability across extensive industrial environments.

By revealing the physical limitations of current wearable components, such as the weight of lithium-ion batteries and the attenuation of high-frequency pulses through concrete slabs, the results of this study serve as guidance for materials research. The need for flexible, conformal electronic substrates to replace rigid PCBs is identified, and passive electromagnetic metamaterials should be developed to mitigate structural reflections and solid-state battery sheets integrated into protective shells.

The developed system enables sensors to be used for real-time tracking, adaptive localization, and automated hazard mitigation. An implementation model for smart occupational safety applications can be constructed on the basis of the developed system, preventing industrial accidents and protecting workers in complex, dangerous work environments.

Acknowledgments

This research was supported by the National Science and Technology Council of Taiwan (Project No.: NSTC 114-2622-E-992-005-).

References

1 J. B. Forsyth, T. L. Martin, D. Young-Corbett, and E. Dorsa: EEE Trans. Autom. Sci. Eng. **9** (2012) 505. https://doi.org/10.1109/TASE.2012.2197390
2 V. Jayasree and M. N. Kumari: Proc. 7th Int. Conf. Smart Structures and Systems (ICSSS, 2020). 1. https://doi.org/10.1109/ICSSS49621.2020.9202138
3 A. Arboleya, J. Laviada, Y. Álvarez-López, and F. Las-Heras: IEEE Antennas Wirel. Propag. Lett. **20** (2021)1794. https://doi.org/10.1109/LAWP.2021.3097136
4 D. K. Amrutha, M. R. Reddy, and R. Vasuki: IJNRD **9** (2024) c491. https://www.ijnrd.org/papers/IJNRD2404288.pdf?utm
5 H. Supriyanto, I. Rokhim, and V. Eliezer: Indones. J. Comput. Sci. **13** (2024) 6032. https://doi.org/10.33022/ijcs.v13i4.4162
6 H. Soganci, S. Gezici, and H. V. Poor: IEEE Wireless Commun. **18** (2011) 19. https://doi.org/10.1109/MWC.2011.5751292
7 IEEE: https://ieeexplore.ieee.org/document/9175063 (Accessed June 2026).
8 N. Xu, M. Guan, and C. Wen: J. Autom. Intell. **4** (2025) 82. https://doi.org/10.1016/j.jai.2025.02.001
9 X. Shen, W. Cheng, and M. Lu: Tsinghua Sci. Technol. **13** (2008) 78. https://doi.org/10.1016/S1007-0214(08)70130-5
10 Y. Cao, C. Chen, D. St-Onge, and G. Beltrame: IEEE Internet Things J. **8** (2021) 13449. https://doi.org/10.1109/JIOT.2021.3066243
11 L. Rana and J. G. Park: IEEE Sens. J. **8** (2024) 31417. https://doi.org/10.1109/JSEN.2024.3441247
12 B. Pinto, Y. Assayag, R. Barreto, and H. Oliveira: IEEE Internet Things J. **13** (2026) 9524. https://doi.org/10.1109/JIOT.2025.3645666
13 A. F. Majeed, R. Arsat, M. A. Baharudin, N. M. A. Latiff, and A. Albaidhani: IEEE Access **13** (2025) 80283. https://doi.org/10.1109/ACCESS.2025.3563815
14 T. Cheng, M. Venugopal, J. Teizer, and P. A. Vela: Autom. Constr. **20** (2011) 1173. https://doi.org/10.1016/j.autcon.2011.05.001
15 A. Schjørring, A. L. Cretu-Sircu, I. Rodriguez, P. Cederholm, G. Berardinelli, and P. Mogensen: Electronics **11** (2022) 3294. https://doi.org/10.3390/electronics11203294
16 L. Bao, K. Li, J. Lee, W. Dong, W. Li, K. Shin, and W. Kim: Sensors **24** (2024) 3341. https://doi.org/10.3390/s24113341
17 A. Nathan, A. Ahnood, M. T. Cole, S. Lee, Y. Suzuki, and P. Hiralal: Proc. IEEE **100** (2012) 1486. https://doi.org/10.1109/JPROC.2012.2190168
18 T. J. Cui, M. Q. Qi, X. Wan, J. Zhao, and Q. Cheng: Light Sci. Appl. **3** (2014) e218. https://doi.org/10.1038/lsa.2014.99
19 Q. Zhang, E. Uchaker, S. L. Candelaria, and G. Cao: Chem. Soc. Rev. **42** (2013) 3127. https://doi.org/10.1039/C3CS00009E